Computation of Raman Scattering Cross Sections in Rare-Gas Crystals. I. Neon and Argon

N. R. Werthamer
Bell Telephone Laboratories, Murray Hill, New Jersey 07974
and
R. L. Gray*
Bell Telephone Laboratories, Murray Hill, New Jersey 07974
and
IBM *Research Laboratories, San Jose, California* 95114
and
T. T. Koehler
IBM *Research Laboratories, San Jose, California* 95114
(Received 14 July 1970)

Two-phonon Raman scattering cross sections are computed for crystals of neon and argon on the basis of a Lorenz dielectric model of the solid and the first-order self-consistent phonon approximation for the lattice dynamics.

I. INTRODUCTION

The technique of Raman scattering as a probe of the structure and excitations of condensed matter has received greatly increased attention[1] in the last several years because of the advent of high-power short-wavelength laser sources. It has become possible to investigate a number of interesting physical situations where previously the scattered intensity would have been too weak for available detectors.

One such class of situations is the Raman scattering from phonons in solid rare-gas crystals where the small polarizability of the rare-gas atoms makes the interaction with light quite weak. A theoretical development has recently been carried out[2] of the one- and two-phonon Raman cross sections to be expected in cubic and hexagonal close-packed helium based on a model of the solid as composed of neutral but dipole-polarizable point masses. Although experiments have not yet been performed on solid helium, an extrapolation[2,3] of the model into the liquid phase yields good qualitative agreement with recent observations of two-roton scattering by Greytak and Yan.[4] A further test of the model would be the observation of two-phonon Raman scattering in the face-centered cubic (fcc) phase of neon or argon. Since light scattering is expected to be somewhat stronger in these materials than in helium (because of the larger atomic polarizability and greater density, partially counterbalanced by the diminished vibrational amplitude), it seems possible that these observations will be attempted in the near future. For this reason, we have extended the theoretical model to fcc neon and argon, and in this paper we present the results of detailed computation of the two-phonon cross sections. In a later paper we intend to present similar results for bcc and hcp helium.

II. PRESENTATION OF RESULTS

We begin by adopting Eq. (31) of Ref. 2 for the two-phonon scattering efficiency at zero temperature. When specialized to the case of Bravais lattices, this is

$$S(\omega) = (N/V)\ (\omega_i/c)^4\ \alpha^4 N^{-1} \sum_{\vec{k}} \sum_{\lambda,\lambda'} (\pi\hbar^2/M^2\omega_{\vec{k}\lambda}\omega_{\vec{k}\lambda'}) \times \delta(\omega - \omega_{\vec{k}\lambda} - \omega_{\vec{k}\lambda'})\ \Big|\sum_{\vec{\tau}} (1 - \cos\vec{k}\cdot\vec{\tau})\, \vec{e}_{\vec{k}\lambda}\vec{e}_{\vec{k}\lambda'} : \langle\nabla\nabla\overleftrightarrow{T}(\vec{\tau})\rangle : \hat{\epsilon}_f\hat{\epsilon}_i\Big|^2 . \quad (1)$$

Reviewing the notation, the crystal is assumed to have N atoms in a volume V, each atom with a polarizability α and mass M. The incident light beam is taken to have angular frequency ω_i and polarization vector $\hat{\epsilon}_i$ and scatters into a polarization ϵ_f with loss of angular frequency ω to the crystal. The crystal has phonon frequencies $\omega_{\vec{k}\lambda}$, assumed undamped, and polarization vectors $\vec{e}_{\vec{k}\lambda}$, characterized by wave vector $\vec{k}$ in the first Brillouin zone and branch index λ. The tensor $\overleftrightarrow{T}(\vec{\tau})$ has the dipolar form

$$\overleftrightarrow{T}(\vec{\tau}) \equiv \frac{\overleftrightarrow{1}}{\tau^3} - \frac{3\vec{\tau}\vec{\tau}}{\tau^5} , \quad (2)$$

and the vectors $\vec{\tau}$ connect mean atomic sites in the crystal. The angular brackets denote average over the phonon zero-point motion

$$\langle f(\vec{\tau})\rangle \equiv \int d^3u \exp[-\tfrac{1}{2}\vec{u}\cdot\overleftrightarrow{D}^{-1}(\vec{\tau})\cdot\vec{u}]\, f(\vec{\tau}+\vec{u}) \Big/ \int d^3u \exp[-\tfrac{1}{2}\vec{u}\cdot\overleftrightarrow{D}^{-1}(\vec{\tau})\cdot\vec{u}] , \quad (3)$$

where

$$\overleftrightarrow{D}(\vec{\tau}) \equiv N^{-1}\sum_{\vec{k}\lambda}(1 - \cos\vec{k}\cdot\vec{\tau})\vec{e}_{\vec{k}\lambda}\vec{e}_{\vec{k}\lambda}/M\omega_{\vec{k}\lambda} . \quad (4)$$

Specializing further to the case of a cubic lattice,

we note that if we write

$$S(\omega) \equiv \hat{\epsilon}_f \hat{\epsilon}_i : \underline{S}(\omega) : \hat{\epsilon}_f \hat{\epsilon}_i \tag{5}$$

in terms of a fourth-rank tensor $\underline{S}(\omega)$, then $\underline{S}(\omega)$ has the same symmetry properties as the elastic constant tensor and hence has no more than three independent elements. We take these to be S_{11}, S_{44}, and S_{12} in the usual Voight notation. Using these symmetry relations in Eq. (5), we can write

$$\begin{aligned} S(\omega) = {} & S_{11}(\omega)\,(\hat{\epsilon}_f \cdot \hat{\epsilon}_i)^2 + S_{44}(\omega)[1 - (\hat{\epsilon}_f \cdot \hat{\epsilon}_i)^2] \\ & + 2[2S_{44}(\omega) + S_{12}(\omega) - S_{11}(\omega)] \\ & \times [\epsilon_{fx}\epsilon_{fy}\epsilon_{ix}\epsilon_{iy} + \epsilon_{fy}\epsilon_{fz}\epsilon_{iy}\epsilon_{iz} + \epsilon_{fz}\epsilon_{fx}\epsilon_{iz}\epsilon_{ix}], \end{aligned} \tag{6}$$

where $\epsilon_{(f,i)\alpha}$ denotes the component of $\hat{\epsilon}_{(f,i)}$ along the αth cube axis. As a byproduct of Eq. (6), we can obtain the dependence on photon polarization in a polycrystalline sample by averaging over all possible orientations of a single crystal:

$$S(\omega)\,|_{\text{poly}} = \tfrac{1}{5}\,[S_{11} + 3S_{44} - S_{12} + (2S_{11} + S_{44} + 3S_{12})(\epsilon_f \cdot \epsilon_i)^2]\ . \tag{7}$$

However, in addition, the dipolar form of $\overleftrightarrow{T}(\vec{\tau})$, Eq. (2), yields immediately

$$\overleftrightarrow{1} : \overleftrightarrow{T}(\vec{\tau}) = 0, \tag{8}$$

$$\overleftrightarrow{1} : \overleftrightarrow{S}(\omega) = 0\ . \tag{9}$$

This latter set of relations in turn leads to the further restriction:

$$S_{12}(\omega) = -\tfrac{1}{2}\,S_{11}(\omega)\ , \tag{10}$$

so that in our point dipole model there are in fact only two independent $\underline{S}(\omega)$ tensor elements, which we take to be $S_{11}(\omega)$ and $S_{44}(\omega)$. An interesting consequence is that the polycrystalline cross section reduces to

$$S(\omega)\,|_{\text{poly}} = \tfrac{3}{5}[\tfrac{1}{2}S_{11}(\omega) + S_{44}(\omega)][1 + \tfrac{1}{3}(\hat{\epsilon}_f \cdot \hat{\epsilon}_i)^2]\ , \tag{11}$$

so that the dependence on photon polarization angles becomes entirely separated from lattice structure (other than that it be cubic) and from dynamics.

We have programmed the numerical evaluation of Eq. (1) on a large-scale digital computer, with the following numerical procedures: (i) The lattice sum on $\vec{\tau}$ includes all atoms within the first twenty shells of nearest neighbors in the fcc lattice. (ii) The reciprocal lattice sum on $\vec{k}$ is taken over a mesh in the first Brillouin zone equivalent through a scale change to all sites in a bcc crystal of cubic shape with 160 atoms on a side. The sum includes 257 000 points in the $\frac{1}{48}$ irreducible portion of the zone. (iii) The continuous variable ω is replaced by a discrete variable ω_j with 200 evenly spaced values between zero and twice the maximum frequency of the phonon spectrum. The energy δ function is then replaced by a step function with value unity if

TABLE I. Parameters chosen for neon and argon.

	Neon	Argon
ϵ	25.41 cm^{-1}	83.05 cm^{-1}
σ	2.781×10^{-8} cm	3.407×10^{-8} cm
Λ	0.0922	0.0296
a	3.156×10^{-8} cm	3.756×10^{-8} cm
α	0.376×10^{-24} cm^3	1.6×10^{-24} cm^3

$$(\omega_j + \omega_{j-1})/2 < \omega_{\vec{k}\lambda} + \omega_{\vec{k}\lambda'} \leqslant (\omega_j + \omega_{j+1})/2$$

and value zero otherwise. (iv) The phonon frequencies and polarization vectors and the phonon averaging as defined by Eqs. (3) and (4) are taken from the first-order self-consistent computation of Gillis, Werthamer, and Koehler. [5]

For this computation, we adopt the Lennard-Jones 6-12 model potential between atoms with parameters ϵ and σ chosen as in Table I so that the calculated ground-state energy and zero-pressure nearest-neighbor distance a match the experimental values. Also listed in Table I are values for the atomic polarizabilities taken from measurements of the index of refraction in the gas phase and for the dimensionless de Boer parameter $\Delta \equiv (\hbar^2/M\epsilon\sigma^2)^{1/2}$.

The results for neon at zero pressure are plotted in Fig. 1, and similarly those for argon in Fig. 2. Both $S_{11}(\omega)$ and $S_{44}(\omega)$ are plotted together, with ω in units of cm^{-1} and the $S(\omega)$ functions in arbitrary units. A physical scale for the $S(\omega)$'s is also in-

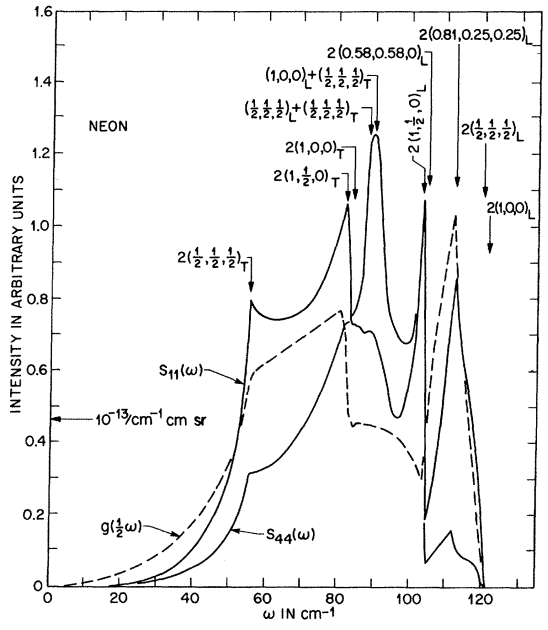

FIG. 1. Two-phonon Raman scattering intensities for neon at zero pressure and temperature as a function of energy loss in cm^{-1}. Critical points in the two-phonon joint density of states are indicated. The one-phonon density of states is also shown.

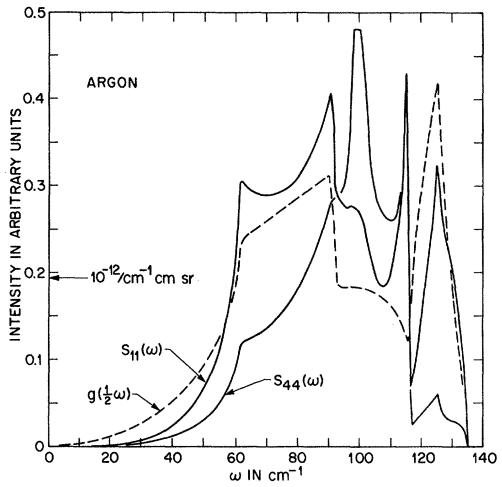

FIG. 2. Same information as in Fig. 1, but for argon.

dicated, in units per wave number per centimeter path length per steradian. Further presented in Figs. 1 and 2 are the phonon densities of states $g(\omega)$ for neon and argon, but expanded over twice the phonon frequency range; i.e., the function

$$g(\tfrac{1}{2}\omega) = N^{-1}\sum_{\vec{k}\lambda} 2\delta(\omega - 2\omega_{\vec{k}\lambda})$$

is plotted as a function of ω. These are included in order to dramatize those critical points in the scattering cross section which are combinations of two different phonon branches. The remaining critical points are easily determined, and their identities are marked in Fig. 1.

It is of some interest to follow the scattering intensities and the critical-point locations as a function of density, since experiments on neon and argon may also be anticipated at elevated pressures. A cursory inspection of Eqs. (1) and (2) might indicate a very pronounced dependence of intensity on nearest-neighbor distance, because of the matrix element varying as a^{-5}. However, the calculations show the total integrated intensities

$$S_{(11,44)} \equiv \int_0^\infty d\omega\, S_{(11,44)}(\omega)$$

to vary only weakly with nearest-neighbor distance, $S \propto a^{+1}$, at least over a range of densities corresponding to pressures up to about 2 kbar because of a strong variation of phonon frequencies with a. In fact, the dominant phonon critical-point frequencies are found to vary as a^{-7} and this dependence is consistent with the linear relation $S \propto a^{+1}$ via Eq. (1). The frequency variation $\omega \propto a^{-7}$ can be understood as reflecting the dominance for phonons near the zone boundary of the repulsive r^{-12} portion of the Lennard-Jones interatomic potential. Longer-wavelength phonons, whose frequencies depend also on the r^{-6} attractive part of the potential and hence whose frequencies have a lesser dependence on density, make very little contribution to the scattering intensities. Because of the simple way in which changes of density affect the predicted Raman cross sections, we do not present plots of the cross sections for any density other than the zero-pressure one of Fig. 1. Table II lists the total integrated intensities for neon and argon at zero pressure.

TABLE II. Integrated intensities [(cm sr)$^{-1}$] for two-phonon raman scattering in neon and argon.

	Neon	Argon
S_{11}	1.07×10^{-11}	7.52×10^{-11}
S_{44}	0.75×10^{-11}	5.28×10^{-11}

*Present address: Department of Music, University of California, Berkeley, Calif. 94720.

[1]See, e.g., *Light Scattering Spectra of Solids*, edited by G. B. Wright (Springer-Verlag, New York, 1969).
[2]N. R. Werthamer, Phys. Rev. 185, 348 (1969).
[3]M. J. Stephen, Phys. Rev. 187, 279 (1969).
[4]T. J. Greytak and J. Yan, Phys. Rev. Letters 22, 987 (1969).
[5]N. S. Gillis, N. R. Werthamer, and T. R. Koehler, Phys. Rev. 165, 951 (1968).